ARPA ORDER NO.: 189-1

R-852-ARPA
September 1971

Numerical Experiments on the Relation Between Microphysics and Dynamics in Cumulus Convection

F. W. Murray and L. R. Koenig

A Report prepared for

ADVANCED RESEARCH PROJECTS AGENCY

Rand
SANTA MONICA, CA. 90406

56

DOCUMENT CONTROL DATA

1. ORIGINATING ACTIVITY	2a. REPORT SECURITY CLASSIFICATION
The Rand Corporation	UNCLASSIFIED
	2b. GROUP ---

3. REPORT TITLE

NUMERICAL EXPERIMENTS ON THE RELATION BETWEEN MICROPHYSICS AND DYNAMICS IN CUMULUS CONVECTION

4. AUTHOR(S) (Last name, first name, initial)

Murray, F. W. and L. R. Koenig

5. REPORT DATE	6a. TOTAL NO. OF PAGES	6b. NO. OF REFS.
September 1971	54	20

7. CONTRACT OR GRANT NO.	8. ORIGINATOR'S REPORT NO.
DAHC15 67 C 0141	R-852-ARPA

9a. AVAILABILITY/LIMITATION NOTICES	9b. SPONSORING AGENCY
	Advanced Research Projects Agency

10. ABSTRACT

A previous numerical model of cumulus growth that treated condensation but not precipitation is modified by the addition of a parameterized treatment of liquid-phase microphysics. This modification improves the realism of the results for several parameters, including maximum height of cloud growth, maximum liquid content, amount and distribution of temperature departure, cloud shape, and occurrence and strength of subcloud downdraft. It is found that one of the most important controlling features in cloud growth is the rate of evaporation of droplets. In particular, the introduction of a class of large particles with a relatively slow evaporation rate produces a smaller temperature deficit at the cloud summit, hence more vigorous cloud growth. In this model, the upper and lower parts of the cloud are, to a large extent, decoupled dynamically; the development of a strong subcloud downdraft by evaporation of precipitation has little effect on the ultimate extent of cloud growth.

11. KEY WORDS

Physics
Weather
Meteorology
Atmosphere
Computer Simulation

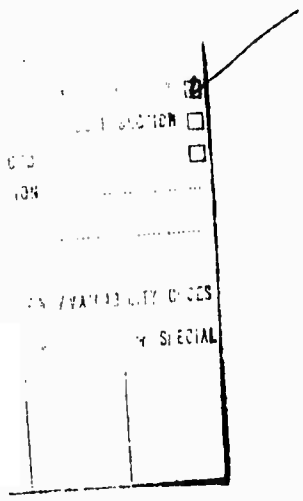

This research is supported by the Advanced Research Projects Agency under Contract No. DAHC15 67 C 0141. Views or conclusions contained in this study should not be interpreted as representing the official opinion or policy of Rand or of ARPA.

ARPA ORDER NO.: 189-1

R-852-ARPA
September 1971

Numerical Experiments on the Relation Between Microphysics and Dynamics in Cumulus Convection

F. W. Murray and L. R. Koenig

A Report prepared for

ADVANCED RESEARCH PROJECTS AGENCY

Rand
SANTA MONICA, CA 90406

PREFACE

Meteorological studies suggest that technologically feasible operations might trigger substantial changes in the climate over broad regions of the globe. Depending on their character, location, and scale, these changes might be both deleterious and irreversible. If a foreign power were to bring about such perturbations either overtly or covertly, either maliciously or heedlessly, the results might be seriously detrimental to the security and welfare of this country. So that the United States may react rationally and effectively to any such actions, it is essential that we have the capability to: (1) evaluate all consequences of a variety of possible actions that might modify the climate, (2) detect trends in the global circulation that presage changes in the climate, either natural or artificial, and (3) determine, if possible, means to counter potentially deleterious climatic changes. Our possession of this capability would make incautious experimentation unnecessary, and would tend to deter malicious manipulation. To this end, the Advanced Research Projects Agency initiated a study of the dynamics of climate to evaluate the effect on climate of environmental perturbations. The present Report is a technical contribution to this larger study.

Rand's activities in numerical modeling of cumulus convection have been reported in a number of publications, of which the most pertinent to the present study are RM-5870-ESSA and RM-5932-NRL. Since cumulus convection represents the major mechanism by which solar energy absorbed at the surface of the earth is transmitted to the upper troposphere, from which it is later transported to regions of energy deficit, this mechanism must be a fundamental consideration in models of the general circulation.

If, in developing a general-circulation model, we were mainly concerned with achieving large-scale patterns that conform reasonably well to those in the real atmosphere, we could, perhaps, simulate cumulus convection in a gross manner, incorporating little physical reality and adjusting various parameters or conditions in any way necessary to force the large-scale features to appear realistic. Any change in the basic

conditions, however, might not properly be taken into account by the parameterization of convection, or the response might be so damped as to be meaningless. But our present goal is to investigate phenomena that might occur as a consequence of the deviation of some quantity from its norm. Therefore, it becomes essential that each component of the model be simulated so as to respond properly to changes in physical conditions upon which it is dependent.

Unfortunately, however, it is impossible to model in detail cumulus convection in a global-circulation model. A parameterization is required. Likewise, because of differences in scale, it is impractical to incorporate details of cloud microphysics in cumulus models. In this work, an attempt is being made to develop realistic microphysical parameterizations for cumulus models with the intention of then developing parameterizations of cumulus convection for the climatic model. By knowing the response of the cumulus model to external stimuli, we hope to develop parameterizations that respond in a similar way to similar stimuli.

SUMMARY

A previously existing numerical model of cumulus growth, treating condensation but not precipitation, is modified by the incorporation of a parameterized treatment of liquid-phase microphysics. This modification improves the realism of the results in several important respects; among them are maximum height of cloud growth, maximum liquid content, amount and distribution of temperature departure, cloud shape, and occurrence and strength of subcloud downdraft. It is found that one of the most important controlling features is the rate of evaporation of droplets. In particular, the introduction of a class of large particles with relatively slow evaporation rate produces a smaller temperature deficit at the cloud summit, hence more vigorous cloud growth. In this model, the upper and lower parts of the cloud are, to a large extent, decoupled dynamically, the development of a strong subcloud downdraft by evaporation of precipitation having little effect on the ultimate extent of cloud growth.

CONTENTS

BLANK PAGE

LIST OF SYMBOLS

The symbols have the following meanings:

$\underset{\sim}{e}_\theta$	azimuthal unit vector
$\underset{\sim}{k}$	vertical unit vector
$\underset{\sim}{v}$	velocity of air parcel
$\underset{\sim}{\omega}$	vorticity
B	buoyancy
D	mesh length
D_b	relative dispersion of drops
E	collection efficiency
L	latent heat of condensation
N_b	initial number concentration of drops
N_o	intercept of Marshall-Palmer curve
R	depth of rainfall
R_d	gas constant for dry air
S_1	rate of condensation
S_2	rate of autoconversion
S_3	rate of collection
S_4	rate of evaporation of precipitation
S_5	net rate of fallout of precipitation
T	temperature
$\overline{T}$	temperature at a given altitude at initial time
T'	departure of temperature from its value at initial time for the given altitude
T'_v	departure of virtual temperature from its value at initial time for the given altitude
T_{vm}	mean value of virtual temperature at initial time over the whole region
V	terminal velocity of water drops
V_o	terminal velocity of water drops at standard temperature and density

$a_1, \ldots, a_6$	parameters used to compute terminal velocity
c_p	specific heat of dry air at constant pressure
c_{pv}	specific heat of water vapor at constant pressure
c_w	specific heat of liquid water
g	acceleration due to gravity
p'	departure of air pressure from its value at initial time for the given altitude
q_v	mixing ratio of water vapor to dry air
q_s	saturation value of q_v
q_c	mixing ratio of suspended water to dry air
q_p	mixing ratio of precipitating water to dry air
r	radial coordinate; also drop radius
t	time
u	radial component of wind
w	vertical component of wind
z	vertical coordinate
δt	time step
ε	ratio of molecular weights of water vapor and dry air
η	azimuthal component of vorticity
θ	azimuthal coordinate
ν_M	eddy diffusion coefficient for momentum
ν_T	eddy diffusion coefficient for temperature
ν_v	eddy diffusion coefficient for water vapor
ν_c	eddy diffusion coefficient for cloud water
ν_p	eddy diffusion coefficient for precipitation water
ρ	air density
ρ_m	mean value of air density at initial time over the whole region
$\bar{\rho}_d$	density of dry air at a given altitude at initial time
$\phi_1, \ldots, \phi_9$	microphysics parameters; see Table 1
ψ	stream function

I. INTRODUCTION

The first generation of two-dimensional numerical models of cumulus convection (Malkus and Witt, 1959; Ogura, 1962) described processes in dry air. This type of model shed some light on the circulations in convective systems, but was unsatisfactory because latent heat is a major source of energy for cumulus clouds. The second generation (Ogura, 1963) incorporated condensation and evaporation of water, but treated the liquid phase as though it were another gas; i.e., microphysical processes involving drops were ignored. Condensed liquid was assumed to move with the air and not to fall out. A considerable degree of realism was attained with this type of model, but there were some obvious shortcomings; among these are the lack of gravitational separation and a rainfall mechanism. Clearly, a more realistic treatment of cloud microphysics is desirable.

One criticism leveled against the model with no fallout of precipitation is that it tends to develop excessively large values of liquid-water content, with consequent "loading" that decreases buoyancy and inhibits cloud growth. A model with fallout could determine the relative dynamic importance of water loading and other processes. But introduction of fallout requires some knowledge of drop-size distribution, which in turn involves a number of microphysical processes.

A number of numerical models of cloud microphysics have been developed (see, e.g., Koenig, 1966), but they cannot readily be combined with the dynamic models because of a gross mismatch of scale and requirement for very large computer capacity. Even so, Arnason, Brown, and Chu (1969) have proposed such a scheme; they have not yet, however, carried it through to completion.

A less ambitious approach to the combination of dynamics and microphysics has been tried, however, with a considerable degree of success. This approach involves the parameterization of microphysical processes in terms of bulk quantities; it was pioneered by Kessler (1967, 1969) in terms of a kinematic cloud model and applied to a dynamic cloud model by Arnason, Greenfield, and Newburg (1968). Numerous other investigators have now adopted parts or all of Kessler's parameterization for use in their cloud models.

The basis for Kessler's parameterization is the conservation of total water substance through a series of continuity and conversion equations. The drop-size spectrum is drastically simplified by dividing the liquid into only two categories: droplets small enough to move with the air and drops large enough to fall relative to the air. These two categories may loosely, but conveniently, be designated suspended water (Kessler refers to this category as "cloud" water) and precipitating water. The precipitating water is assumed to have the drop-size distribution described by Marshall and Palmer (1948), but all drops are assumed to fall relative to the air with the terminal velocity appropriate to the volume-median drop size.

There are two processes by which suspended water can be converted to precipitation water. The first is autoconversion, which is a coalescence of small droplets; this depends on the bulk density of suspended water. The second is collection, which is a coalescence of large and small drops due to their differential velocity, this depends on the bulk densities of both suspended water and precipitating water. Kessler also parameterized the evaporation of precipitating water when it enters an undersaturated region. Since this occurs at a finite rate, it is possible for liquid water to continue to exist even though the air is not saturated.

Portions of Kessler's parameterization have been used successfully in several one-dimensional cloud models (e.g. Simpson and Wiggert, 1969, Weinstein, 1969), and some of the effects of varying the parameters and equations have been discussed. The application to two dimensions poses some additional problems, but it has been accomplished by Arnason, Greenfield, and Newburg (1968) and by Liu and Orville (1969) using a version of the parameterization proposed by Srivastava (1967). However, no specific study of the way the inclusion of parameterized microphysics affects a two-dimensional model has been published. It is the purpose of this paper to fill this gap and, by making use of the results obtained thereby, to infer something about the nature of the growth and decay of real cumulus clouds.

II. MATHEMATICAL DESCRIPTION OF THE MODEL

The basis for the model used in the present experiment is the two-dimensional nonprecipitating model described by Murray (1970). However, in accordance with Kessler's scheme for treating microphysical processes, the liquid water has been divided into suspended and precipitating water. The processes of evaporation and condensation treated by the old model now describe conversions between vapor and suspended water, and their rate is such that the air can never be undersaturated in the presence of suspended water nor supersaturated. In addition, suspended water may be transformed to precipitating water by autoconversion and collection, and precipitating water falls relative to the air (but moves with the air horizontally) and evaporates at a slower rate than suspended water.

The Boussinesq approximation is used, so the equation of motion is

$$\frac{\partial \underset{\sim}{v}}{\partial t} = -\underset{\sim}{v} \cdot \nabla \underset{\sim}{v} - \frac{1}{\rho_m} \nabla p' + g\left(\frac{T_v'}{T_{vm}} - q_c - q_p\right)\underset{\sim}{k} + \nu_M \nabla^2 \underset{\sim}{v} \qquad (1)$$

and the continuity equation is

$$\nabla \cdot \underset{\sim}{v} = 0 \qquad (2)$$

Let

$$B = g\left(\frac{T_v'}{T_{vm}} - q_c - q_p\right) \qquad (3)$$

This expresses the buoyancy force, consisting of three parts: First, the buoyancy depends on the departure of virtual temperature (that is to say, of density of the moist air) from its basic state. Second, it depends on the weight of the suspended water. Since this water moves with the air, its weight represents a simple downward force on

the parcel of which it is a part. Third, it depends on the weight of the precipitating water. This water is moving downward relative to the air parcel at its terminal velocity, which by definition is that speed at which the aerodynamic drag is exactly balanced by the weight. Hence, the downward force of the relatively falling drops takes the same form as the downward force of the relatively stationary droplets.

If we substitute Eq. (3) into Eq. (1), take the curl, and make use of Eq. (2), we get the vorticity equation

$$\frac{\partial \underset{\sim}{\omega}}{\partial t} = \nabla \times (\underset{\sim}{v} \times \underset{\sim}{\omega}) + \nabla \times B\underset{\sim}{k} - \nu_M \nabla \times (\nabla \times \underset{\sim}{\omega}) \tag{4}$$

where $\underset{\sim}{\omega} = \nabla \times \underset{\sim}{v}$. In cylindrical coordinates (r, θ, z), with the assumption of axial symmetry and no rotation, Eq. (4) becomes

$$\frac{\partial \eta}{\partial t} = -\left[\frac{\partial}{\partial r}(u\eta) + \frac{\partial}{\partial z}(w\eta)\right] - \frac{\partial B}{\partial r} + \nu_M \left(\frac{\partial}{\partial r}\left[\frac{1}{r}\frac{\partial}{\partial r}(r\eta)\right] + \frac{\partial^2 \eta}{\partial z^2}\right) \tag{5}$$

Here the horizontal and vertical components of wind are defined by a stream function, ψ, according to

$$\left.\begin{aligned} u &= -\frac{1}{r}\frac{\partial \psi}{\partial z} \\ w &= \frac{1}{r}\frac{\partial \psi}{\partial r} \end{aligned}\right\} \tag{6}$$

and the tangential component of vorticity is

$$\eta = -\left(\frac{\partial w}{\partial r} - \frac{\partial u}{\partial z}\right) = -\frac{1}{r}\left[r\frac{\partial}{\partial r}\left(\frac{1}{r}\frac{\partial \psi}{\partial r}\right) + \frac{\partial^2 \psi}{\partial z^2}\right] = \underset{\sim}{e}_\theta \cdot \nabla \times \underset{\sim}{v} = \underset{\sim}{e}_\theta \cdot \underset{\sim}{\omega} \tag{7}$$

Except for fallout and eddy diffusion, the total water is individually conserved. Hence

$$\frac{dq_v}{dt} = -S_1 + S_4 + \nu_v \nabla^2 q_v \tag{8}$$

$$\frac{dq_c}{dt} = S_1 - S_2 - S_3 + \nu_c \nabla^2 q_c \tag{9}$$

$$\frac{dq_p}{dt} = S_2 + S_3 - S_4 - S_5 + \nu_p \nabla^2 q_p \tag{10}$$

where S_1 is the rate of condensation, S_2 is the rate of autoconversion, S_3 is the rate of collection, S_4 is the rate of evaporation of precipitating water, and S_5 is the net rate of fallout. It has generally been found desirable to let $\nu_p = 0$, but $\nu_v = \nu_c \neq 0$ in order that turbulent entrainment be effective.

The thermodynamic equation is

$$\frac{dT'}{dt} = \frac{L\,(S_1 - S_4)}{c_p + q_v c_{pv} + (q_c + q_p)c_w} - \frac{gw}{c_p} - \frac{d\bar{T}}{dz} + \nu_T \nabla^2 T' \tag{11}$$

As in the nonprecipitating model of Murray (1970), the rate of condensation is

$$\left.\begin{aligned} S_1 &= \frac{1 - \dfrac{c_p T - L q_s}{\varepsilon L}}{L + \dfrac{c_p R_d T^2}{L q_s (\varepsilon + q_s)}}\, gw && ;\ q_v = q_s \\ S_1 &= 0 && ;\ q_v < q_s \end{aligned}\right\} \tag{12}$$

If $w < 0$, then S_1 is the rate of evaporation of suspended water. In this case, the total evaporation during a time step may not exceed in

magnitude the initial value of q_c for that time step. Care is taken that the condition $q_v > q_s$ never exist when Eq. (12) is to be solved.

The rate of autoconversion, according to Kessler, is

$$\left.\begin{aligned} S_2 &= \phi_1(q_c - \phi_2/\bar{\rho}_d) && ; \; q_c > \phi_2/\bar{\rho}_d \\ S_2 &= 0 && ; \; q_c \leq \phi_2/\bar{\rho}_d \end{aligned}\right\} \tag{13}$$

(The recommended values of the parameters ϕ_i are given in Table 1.) In this formulation, autoconversion does not occur unless q_c exceeds a certain threshold value. Berry (1968) has proposed an alternative formulation that does not have this property; it is

$$S_2 = \frac{\phi_7 \bar{\rho}_d q_c^2}{1 + \dfrac{\phi_8}{\bar{\rho}_d q_c}} \tag{14}$$

There is reason to believe that Berry's formulation for autoconversion, being based on more accurate coalescence equations, is better than Kessler's. Simpson and Wiggert (1969) have used it with two sets of parameters, one for clouds over land and one for clouds over water. All three formulations have been used in the present study.

The rate of collection is

$$S_3 = \phi_3 \, q_c \, (\bar{\rho}_d q_p)^{0.875} \tag{15}$$

The rate of evaporation of precipitating water is

$$\left.\begin{aligned} S_4 &= \phi_4 \, (q_s - q_v)(\bar{\rho}_d \, q_p)^{0.65} && ; \; q_v < q_s \\ S_4 &= 0 && , \; q_v \geq q_s \end{aligned}\right\} \tag{16}$$

Table 1

VALUES OF MICROPHYSICAL PARAMETERS (S. I. UNITS)

$\phi_1 = 10^{-3}\,\text{sec}^{-1}$

$\phi_2 = 0.5 \times 10^{-3}\ \text{kg m}^{-3}$

$\phi_3 = 6.96 \times 10^{-4}\ E\ N_o^{0.125} \times 10^{2.625}$

$\phi_4 = 1.93 \times 10^{-6}\ N_o^{0.35} \times 10^{1.95}$

$\phi_6 = -38.3\ (1000/N_o)^{0.125}$

$\phi_7 = 10/3$

$\phi_8 = 7.32 \times 10^{-6}\ N_b/D_b$

$\phi_9 = 4.35 \times 10^{4}\ (1000/N_o)^{0.25}$

$N_o = 10^7$ (intercept of Marshall-Palmer curve)

$N_b =$ { 50 (maritime); 2000 (continental) } (initial number concentration of drops)

$D_b =$ { 0.366 (maritime); 0.146 (continental) } (relative dispersion of drops)

$E = 1$ (collection efficiency)

The net rate of fallout of precipitating water, S_5, cannot readily be expressed in the same Lagrangian manner as the other terms. It has been found expedient to solve Eq. (10) with S_5 omitted, and then to correct the result for fallout; this is discussed at greater length in paragraph (g) of Section IV. Whatever the method used to evaluate S_5, however, the terminal velocity of the volume-median water drop must be known. Kessler suggests the relation

$$V = \phi_6 \, (\bar{\rho}_d \, q_p)^{0.125} \tag{17}$$

Note that by convention $V \leq 0$. Kessler also suggests a correction for altitude, amounting to some 24 percent at 600 mb, that could be incorporated into Eq. (17). After several runs were made using Eq. (17), it was noted that when q_p is large, Eq. (17) gives errors in excess of 10 percent with respect to the sea-level observations of Gunn and Kinzer (1949). At intermediate values, the error is smaller, but for very small values of q_p, the error can be several hundred percent. Of course, not much water is involved when the q_p is small; however, it was deemed desirable to find a better expression for V than Eq. (17).

By a process of curve fitting, Wobus has matched the experimental values of Gunn and Kinzer to a high degree of accuracy (Wobus, Murray, and Koenig, 1971). First, the drop radius (in μm) is determined. According to Kessler, this is

$$r = \phi_9 \, (\bar{\rho}_d \, q_p)^{0.25} \tag{18}$$

From this, the terminal velocity (in m sec^{-1}) at sea level is found by means of

$$
\left.
\begin{aligned}
r \le 50: \quad V_0 &= -1.197 \times 10^{-4}\, r^2 + \\
&\quad 8.64 \times 10^{-11}\, r^5 + \\
&\quad 1.44 \times 10^{-13}\, r^6 \\
50 < r \le 230: \quad V_0 &= -9 \times 10^{-3}\, r + 0.18 \\
230 < r \le 450: \quad V_0 &= -0.008r - 0.07 + a_1 \\
450 < r: \quad V_0 &= 5.545/a_3 - 9.215 + a_1
\end{aligned}
\right\} \qquad (19)
$$

where

$$a_1 = 0.4/(r - 210)$$

$$a_2 = r - 450$$

$$a_3 = 2.036791 \times 10^{-15}\, a_2^5 - 3.815343 \times 10^{-12}\, a_2^4 + 4.516634 \times 10^{-9}\, a_2^3 - 8.020389 \times 10^{-7}\, a_2^2 + 1.44274121 \times 10^{-3}\, a_2 + 1$$

Finally, the terminal velocity appropriate to the actual density and viscosity of the air is found by means of

$$V = a_5 - [a_5^2 + a_6]^{1/2} \qquad (20)$$

where

$$a_4 = \rho[0.2177076r/V_0 + 1817.8/r]/V_0$$

$$a_5 = 6[775.7257 - 719813.4/(T + 918.768)]/ra_4$$

$$a_6 = 0.261249r/a_4$$

In all the runs described herein, Eq. (20) was used in preference to Eq. (17).

In the microphysical equations of this paper, mixing ratios are multiplied by $\bar{\rho}_d$. This is because the original parameterization was developed in terms of bulk density (mass of water per unit volume of dry air), whereas the hydrodynamic equations are in terms of mixing ratio (mass of water per unit mass of dry air). An extremely small error is incurred by using the initial density at the specified altitude rather than the current density.

III. BOUNDARY AND INITIAL CONDITIONS

The principal boundary conditions are the assumption of axial symmetry about the line r = 0, and of rigid, free-slip boundaries at the outer, lower, and upper limits.

Initially the air is assumed to be at rest and horizontally homogeneous, and to contain no liquid water. In the present study the basic sounding (San Juan, Puerto Rico, 2300 GMT, 20 August 1963) and the initial impulse used to start the convection were identical to those in the previous study by Murray (1970).

The model space was a cylinder of radius 6 km and depth 9 km. Comparison with a run having a ceiling of 7 km showed no significant differences, indicating that except in Run 6, which is not realistic in any case, there is no adverse interaction between the cloud and the upper boundary. The outer boundary is even more remote in a dynamical sense.

Special effort has been made to assure the conservation of total mass of water. In general this is accomplished to within 0.2 percent for 60 minutes of simulated time (~ 450 time steps).

IV. METHOD OF SOLUTION

Within any time step, the order of operations is as follows:

(a) The vorticity equation, Eq. (5), is solved for η at the new time. An Eulerian scheme is used, with centered differences in both space and time.

(b) By relaxation, ψ is found from η, using Eq. (7), and then u and w are calculated by means of Eq. (6).

(c) For each grid point, an upstream point is found such that the air parcel at the upstream point at the beginning of the time step moves to the grid point at the end of the time step. The initial value of each variable (T', q_c, q_p, etc.) is found at the upstream point by bilinear interpolation. For the sake of internal consistency, some variables are not interpolated directly but are calculated from other interpolated variables.

(d) If $q_v > q_s$ at the upstream point, enough suspended water is condensed instantaneously to bring the air to exact saturation. This alters the values of q_v, q_c, q_s, and T'. If $q_v < q_s$ and $q_c > 0$, evaporation of suspended water occurs in the same manner, but not to exceed q_c. If, following the latter check and correction, $q_v < q_s$, step (e) is skipped.

(e) Using current values of all variables, S_1, S_2, and S_3 are determined. These values are used in conjunction with Eqs. (8) through (11) to get intermediate new values for q_v, q_c, q_p, and T'.

(f) The eddy-diffusion terms of Eqs. (8) through (11) and the terms $-gw/c_p$ and $-d\bar{T}/dz$ of Eq. (11) are incorporated into the intermediate values.

(g) Terminal velocity, V, is computed from Eq. (20), and the intermediate value of q_p determined in step (e) for the grid point, under the assumption that precipitating water moves with the air, is now assumed to apply to a point a distance of $|V\delta t|$ below the grid point. Under the assumption of linear variation of $\bar{\rho}q_p$ from one datum point to another, the new value of q_p at the grid point of height z_0 is found by solution of

$$q_p(z_0) = \frac{1}{D\bar{\rho}(z_0)} \int_{z_0-D/2}^{z_0+D/2} \bar{\rho} q_p \, dz \tag{21}$$

where D is the mesh length. If z_0 is the highest level for which $q_p(z_0+V\delta t) > 0$, then it is assumed that $q_p(z_0+D/2) = 0$; this suppresses the artificial upward migration of the top of the cloud. At $z = 0$, Eq. (21) is modified to

$$q_p(0) = \frac{2}{D\bar{\rho}(0)} \int_0^{D/2} \bar{\rho} q_p dz \tag{22}$$

and the mass of water per unit horizontal area falling out as rain is

$$R = \int_{V(0)\delta t}^{0} \bar{\rho} \, q_p dz \tag{23}$$

As it happens, this mass in kilograms is equal to the rain depth in millimeters. (In this Report, the term "rain" refers to water that has fallen to the ground.) The procedure outlined above is almost exactly conservative of the sum of precipitating water and rain water. The percent difference in the total mass of precipitating and rain water in a column before and after the computation is typically of the order of 10^{-14} percent.

(h) The instantaneous correction of step (d) is again applied. This does not represent a physical process, but a compensation for errors introduced by linear computation of nonlinear processes. The adjustment is slight.

(i) If $q_v < q_s$ and $q_p > 0$, S_4 is computed, and the values of q_v, q_p, and T' are appropriately adjusted through Eqs. (8), (10), and (11).

V. SOME RESULTS OF THE RUNS

In order to determine the effects of several variations in the parameterization, six runs were made. All six had the same initial sounding and impulse (also used in the study by Murray, 1970), and in all cases the eddy-diffusion coefficients were $\nu_M = \nu_T = \nu_v = \nu_c = 40\ m^2\ sec^{-1}$; $\nu_p = 0$. The principal characteristics of the runs were as follows:

Run 1. The Kessler parameterization was used as described herein, except that the autoconversion threshold was made excessively high ($\phi_2 = 5 \times 10^4$ kg m^{-3}). Consequently, no precipitating water could appear. This is essentially the same as the axisymmetric run described by Murray (1970), but small variations in the programs make them not quite identical.

Run 2. The Kessler parameterization was used without modification. The autoconversion threshold was normal ($\phi_2 = 0.5 \times 10^{-3}$ kg m^{-3}).

Run 3. This run was identical with Run 2 except that Berry's expression for autoconversion, Eq. (14), was used in place of Kessler's, Eq. (13). The parameters entering into ϕ_8 were those appropriate for clouds in a maritime air mass (see Appendix B).

Run 4. This run was identical to Run 3, except that the parameters entering into ϕ_8 were those appropriate for clouds in a continental air mass.

Run 5. This run was identical to Run 3, except that Eq. (16) was modified to permit total evaporation of q_p within one time step provided that it did not make $q_v > q_s$.

Run 6. This run was identical to Run 3, except that in any process involving evaporation, the latent heat was set equal to zero. In any process involving condensation, it had its usual value.

Comparison of Run 1 with the others shows the effects of the change from a second-generation model (with condensation but no accounting for drop size) to a third-generation model (accounting for drop size in a simplified manner). Comparisons of Runs 2, 3, and 4 show, among other things, the effects of varying the rate at which large drops are produced,

especially in the early stages. Runs 5 and 6 were added to test a hypothesis concerning evaporation that was suggested by the other runs.

A summary of some results of the six runs is given in Table 2. All tabulated values except cloud efficiency and dissipation time refer to the central axis. Rainfall rates and amounts are area-weighted means for the axis and the first grid point away from it. Not surprisingly, the extreme values of the several variables are almost always found on the central axis. One notable exception is the negative temperature departure near the cloud summit, which occasionally reaches its greatest magnitude a grid unit or two away from the axis and a little below the level of the summit on the axis. This, perhaps, is merely an apparent feature, resulting from the inability of the finite-difference mesh to resolve the small-scale patterns of temperature departure; note Figs. 10 through 13, on pages 32 through 35.

Perusal of Table 2 shows that in several respects the three runs with normal precipitation development (Runs 2, 3, and 4) are similar, but collectively they differ markedly from Run 1, which has no precipitation. Among these properties are maximum cloud height (which is 1400 to 1800 m greater with precipitation than without), extreme downdraft at 200 m (which is negligible without precipitation, but considerable with), summit temperature departure (which is somewhat greater without precipitation than with), and time of dissipation (which is considerably earlier without precipitation than with). On the other hand, some properties, such as maximum liquid-water content and maximum updraft strength, show no such clear-cut distinction.

1. Partition of Total Water

The differences in maximum cloud-top height, as well as some other indices, suggest that some phenomenon associated with the inclusion of a fallout mechanism for liquid water results in more vigorous cloud growth. This is further borne out by Figs. 1 through 4, which show the variation with time of the total mass of water of each category (except vapor) in the computational domain. Two supplementary curves in these figures are for total airborne liquid water (the sum of suspended and precipitating water) and total liquid (the sum of total airborne and

Table 2

SUMMARY OF CLOUD CHARACTERISTICS

RUN NUMBER →	1	2	3	4	5	6
PRECIPITATION →	No precipitation	Unmodified Kessler	Kessler with Berry autoconversion (maritime)	Kessler with Berry autoconversion (continental)	Kessler-Berry (maritime) with instantaneous evaporation of precipitation	Kessler-Berry (maritime) with no cooling due to evaporation
MAXIMUM CLOUD TOP						
Height (m)	4000	5600	5800	5400	4000	8800**
Time (min)	32	36	37	35	33	26
MAXIMUM LIQUID WATER						
Amount (g kg^{-1})	4.73	4.90	5.02	4.69	4.37	16.20
Height (m)	3800	2900	3000	3000	2800	6800
Time (min)	32	31	31	31	31	32
MAXIMUM UPDRAFT						
Strength (m sec^{-1})	15.34	13.93	15.07	14.42	12.65	20.34
Height (m)	3400	3600	3600	3400	3200	8400
Time (min)	30	30	30	30	29	31
MAXIMUM DOWNDRAFT						
Strength (m sec^{-1})	-0.092	-4.95	-5.03	-5.10	-11.01	-2.19
Time (min)	16	37	37	37	38	29
Time to reach -0.1 m sec^{-1} (min)	--	20	15	28	16	16
RAINFALL AT AXIS						
Maximum rate* (mm min^{-1})	--	0.500	0.525	0.481	0.268	2.425***
Time (min)	--	36	36	37	34	40
Total* (mm)	--	6.4	7.7	4.8	2.2	30.0***
Time first reaches ground (min)	--	19	16	24	29	15
Maximum cloud efficiency (percent)	--	68	82	50	25	17***
SUMMIT TEMPERATURE DEPARTURE						
Extreme (°C)	-2.77	-1.38	-1.72	-1.60	-2.24	-1.07
Time (min)	31	26	29	35	32	23
CLOUD DISSIPATION						
Time (min)	53	75	76	74	43	>40

* Integrated over a disk 300 m in radius.

** Cloud reached top of computational space.

*** Computation was terminated at 40 minutes.

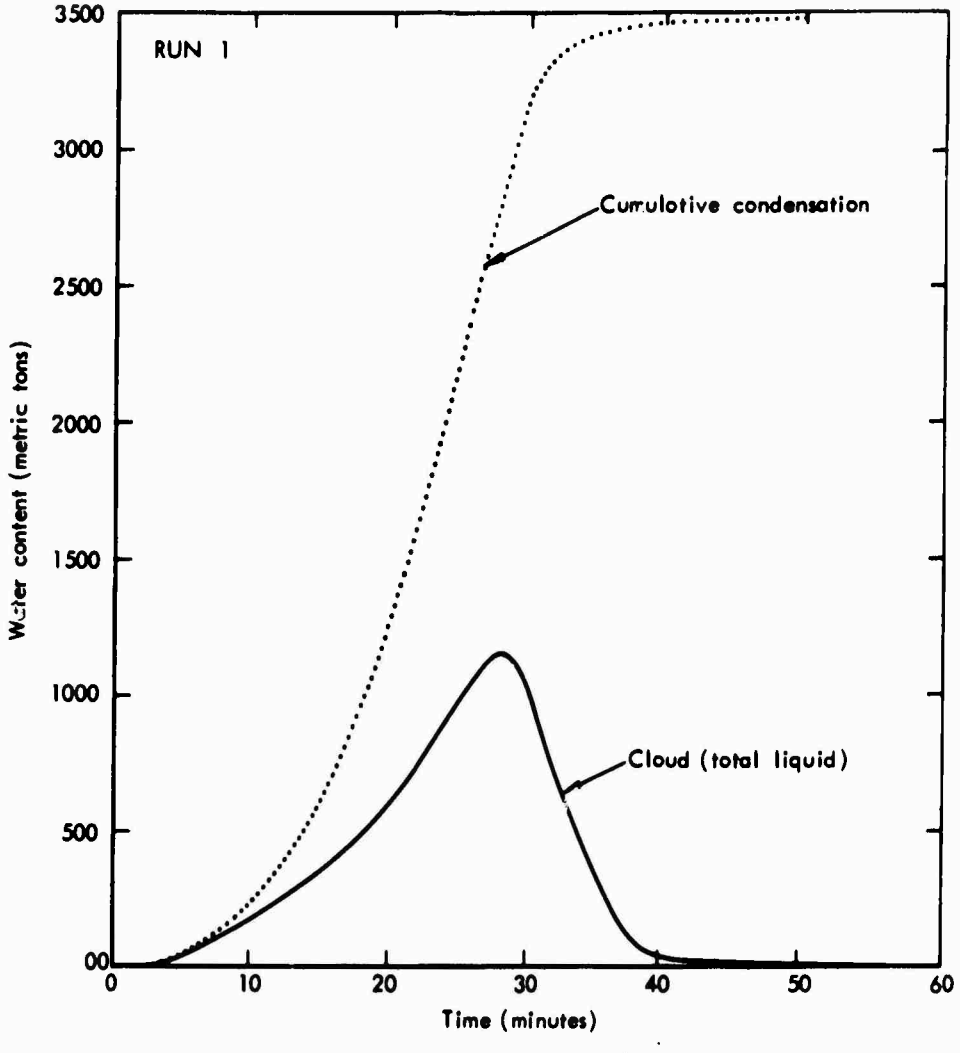

Fig. 1 -- Total liquid water and cumulative amount of water condensed *versus* time, Run 1. (All liquid water is in the form of suspended droplets.)

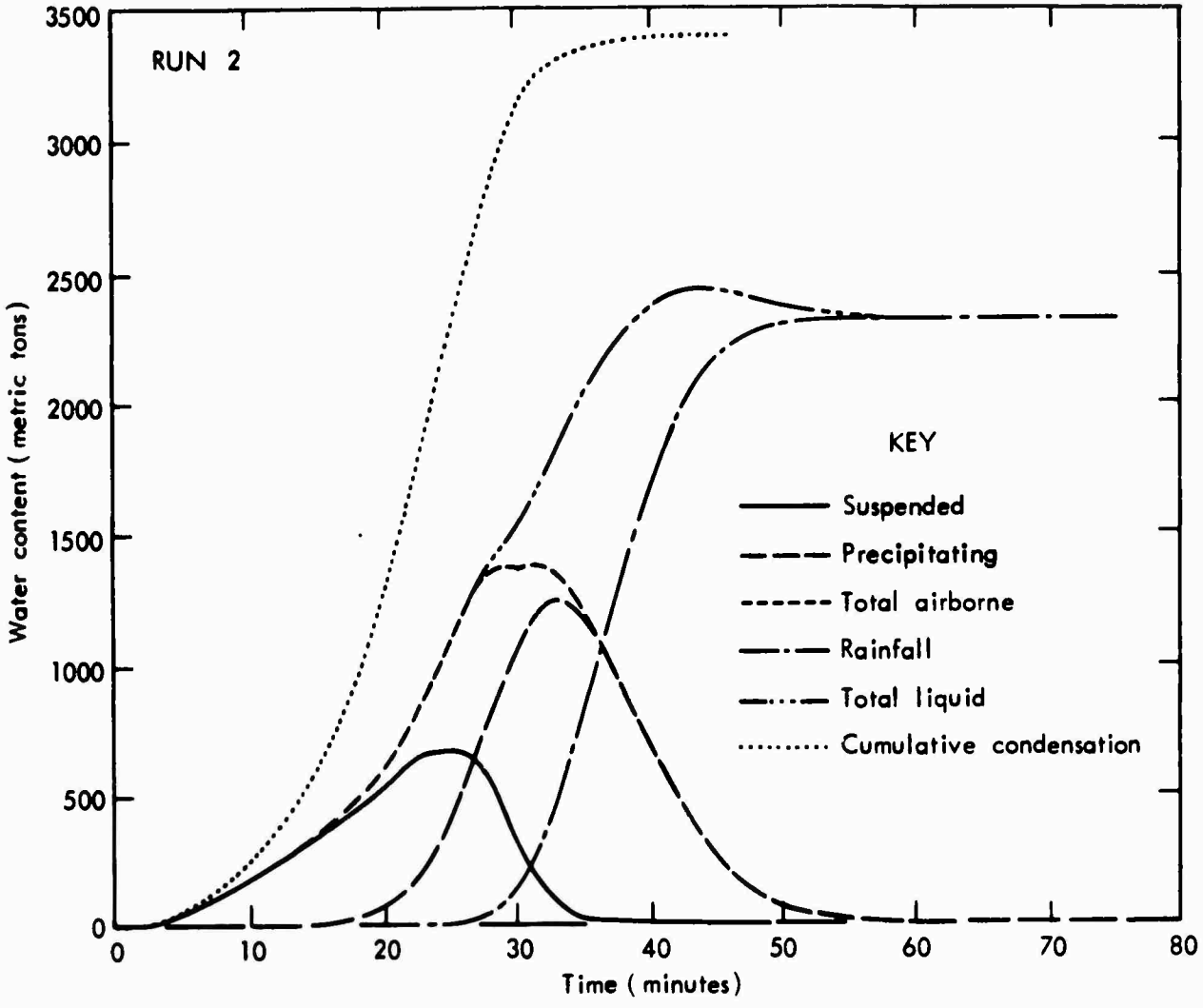

Fig. 2 -- Total liquid water in each form and cumulative amount of water condensed *versus* time, Run 2.

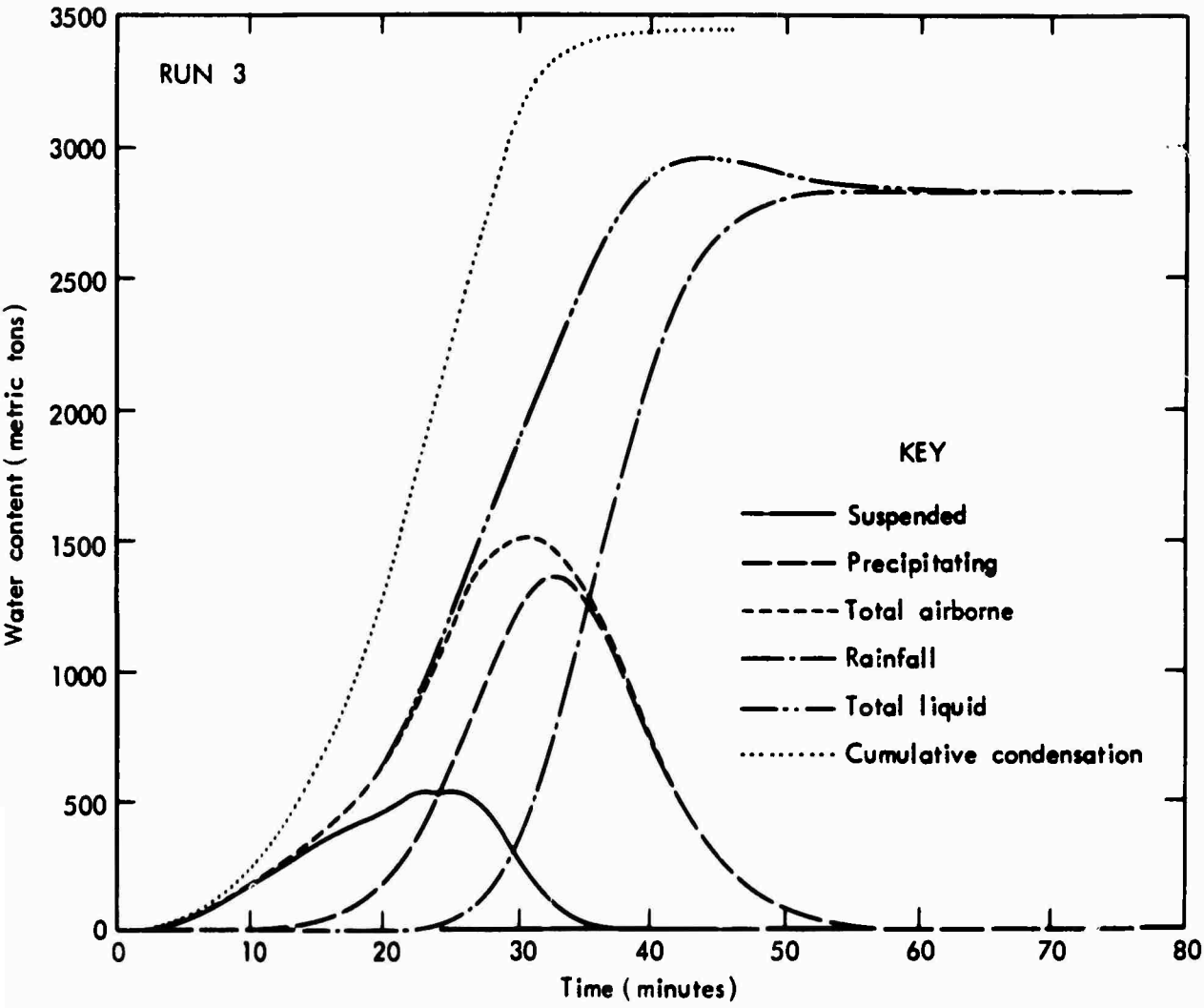

Fig. 3 -- Total liquid water in each form and cumulative amount of water condensed *versus* time, Run 3.

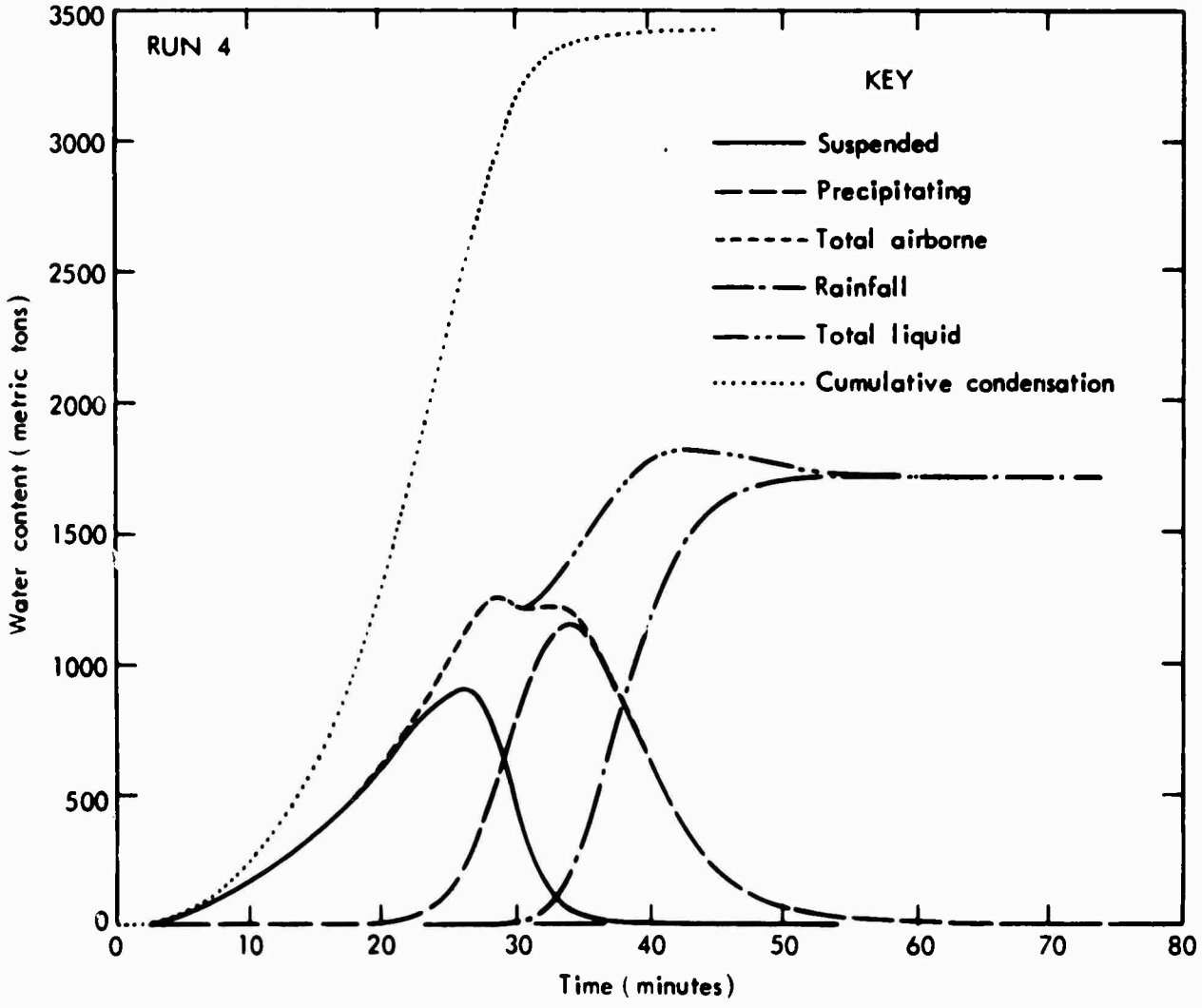

Fig. 4 -- Total liquid water in each form and cumulative amount of water condensed *versus* time, Run 4.

fallen rain). In Fig. 1, of course, the curves of suspended water and total liquid are identical. Figures 2, 3, and 4 all show substantially more liquid than Fig. 1, confirming the impression of greater activity. Paradoxically, however, the curves of cumulative condensation, or total mass of water condensed up to a given time, are almost identical in all four figures. This would suggest that it is not merely the innovation of allowing some of the condensed water to fall relative to the air that affects the dynamics of the cloud.

It has been proposed that the nonprecipitating model, by requiring the condensate to be carried with the air, contains an extra loading factor that decreases the buoyancy and damps the cloud development. This mechanism is probably at work, even though Table 2 shows higher liquid-water content for Runs 2 and 3 than for Run 1. It will be noted that the maximum of liquid-water content occurs near the top of the cloud in Run 1, well above the level of maximum updraft, but in Runs 2, 3, and 4 it occurs much lower, despite a much higher cloud top. (Note also Figs. 6 and 7, pages 26 and 27.) It is, in fact, well below the level of maximum updraft, which is about the same in all four runs. If computed soundings are plotted on a thermodynamic diagram, it is found that the nonprecipitating model develops essentially an adiabatic profile of total water content on the central axis, but the precipitating models develop profiles that exceed the adiabatic at lower levels and are exceeded by it at higher levels. Thus, as expected, the nonprecipitating model has its heaviest water loading near the top, where it evidently is most effective in damping cloud development, whereas the precipitating models have it in the lower levels, where it has less effect.

2. Evaporation

Although loading is important, the computational results indicate that there is a much more powerful mechanism at work to differentiate between Run 1 and Runs 2, 3, and 4. This mechanism is evaporation. In all four models, suspended water is assumed to consist of droplets so small that they can evaporate virtually instantaneously, and so they cannot persist from one time step to the next where the air is subsaturated. On the other hand, precipitating water consists of larger drops

having finite evaporation rates. Accordingly, these drops do not necessarily completely evaporate in one time step, even though the air remains subsaturated. Consequently, the cooling associated with evaporation proceeds more slowly. The importance of the rate of evaporation is pointed up by Runs 5 and 6, which are both basically like Run 3, but which have certain artifical conditions imposed on them. Run 5 illustrates rapid evaporation by allowing precipitating water in a subsaturated volume to evaporate instantaneously, as does suspended water. Thus the dynamics of the cloud are influenced more rapidly by the thermal effects of evaporation in a subsaturated volume, but gravitational effects are unchanged. Run 6 illustrates the opposite extreme. Both condensation and evaporation proceed as in Run 3, but the latent heat of evaporation is taken to be zero. Thus the dynamical consequences of evaporative cooling (but not of condensational warming or of water loading) are suppressed. The results are highly unrealistic, but when taken together with the results of the other runs, they illuminate some of the important dynamical processes.

Because precipitating water was allowed to fall, the maximum of liquid water content in Run 5 (instantaneous evaporation) occurred at the same low level as in Runs 2, 3, and 4, but its value was less. The maximum height of the cloud top, however, was the same as in the non-precipitating model and much lower than in the other precipitating models. There are at least two consequences of the method of treating evaporation that contribute to this effect. First, since precipitating particles in Runs 2, 3, and 4 can exist in a subsaturated environment, subsaturated air volumes formed by mixing cloudy air and ambient air can contain sufficient precipitating drops to be described as cloudy air; whereas, if only suspended droplets are initially present, evaporation would result in clear air. In essence, allowing finite evaporation rates decreases the rate of erosion due to entrainment, whereas instantaneous evaporation promotes erosion and dissipation of the cumulus tower. Second, and we believe more important, the temperature departure from the ambient value near the cloud top is markedly influenced by the amount of local evaporation. This, in turn, markedly influences the buoyancy. Because of the greater rate of evaporation, air near the top

of a nonprecipitating or instantly evaporating cloud becomes colder and more dense than that associated with a normal precipitating cloud. This is borne out by the summit temperature departures shown in Table 2.

By contrast, the temperature deficit near the summit in Run 6 (zero heat of evaporation) was considerably smaller than that in the other runs. (The extreme value shown in Table 2 is atypical; most of the time the deficit was smaller yet.) The cloud responded by growing excessively, soon reaching the top of the computational space despite water loading three times as great as in the other runs. This is clear evidence that evaporational cooling has more dynamic effect than water loading.

3. Subcloud Downdraft

Effects near the summit, however, cannot account for all of the significant differences among the runs; hence there are other important consequences of the method of treating evaporation. Most notable is the total amount of water condensed. As has been mentioned, this was almost identical for Runs 1 through 4, but, as shown in Fig. 5, it was much smaller for Run 5 (instantaneous evaporation). Also, the maximum updraft was smallest for Run 5, but largest for Run 1 (disregarding Run 6). Apparently a precipitating cloud with instant evaporation is in some important way different in its dynamics from a normal precipitating cloud or a nonprecipitating cloud. An explanation is suggested by the downdraft below the cloud. In Run 1, liquid water could not fall below the cloud base, there to evaporate, and by cooling the air initiate a strong downdraft. By contrast, in Runs 2, 3, and 4, evaporation of falling precipitation led to a downdraft of about 5 m sec^{-1}. The more rapid evaporation of Run 5 led to a downdraft of 11 m sec^{-1}. One might argue that the strong downdraft of Run 5 cut the cloud off from its main source of moisture, inhibited its growth, and led to its early dissipation, but this argument is not valid, as comparison of Runs 2, 3, and 4 with Run 1 will show. In this comparison, Run 1, with the weakest downdraft, also had the least vertical development. On the other hand, the downdraft must have some inhibiting effect on cloud growth, for Run 5, with its strong downdraft below cloud base, condensed less water and

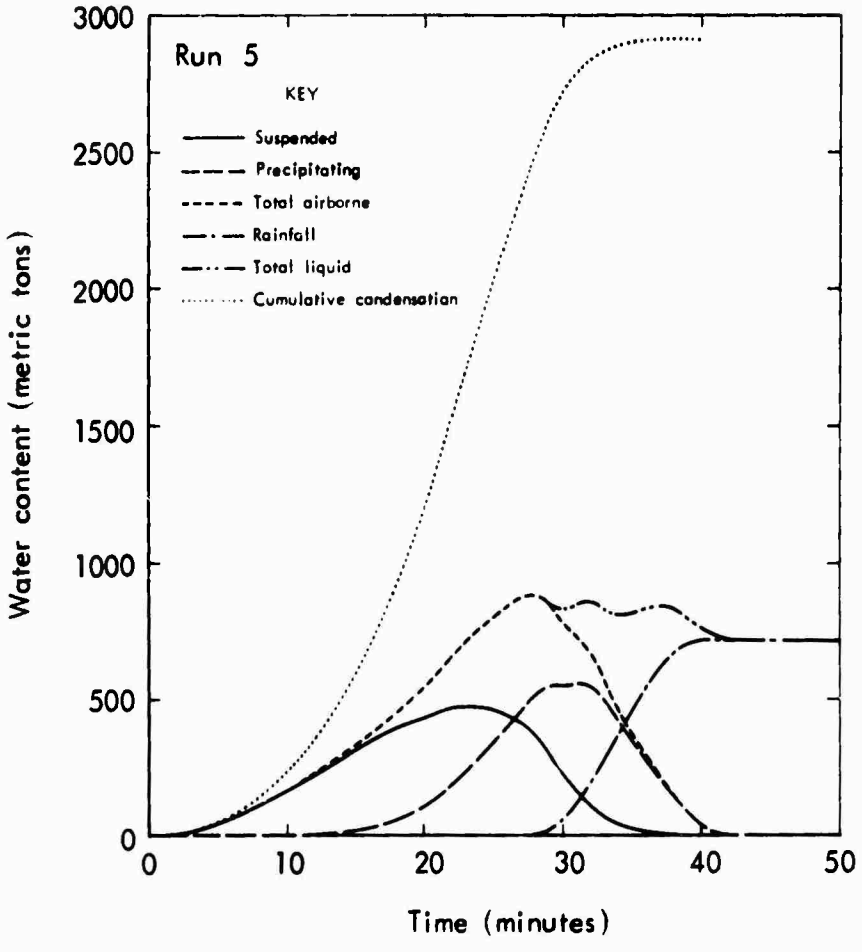

Fig. 5 -- Total liquid water in each form and cumulative amount of water condensed *versus* time, Run 5.

dissipated earlier than Run 1, with negligible downdraft. Interestingly, Run 6 developed a moderate downdraft below the cloud. Since evaporative cooling was not operative, water loading might be the cause. It should be noted, though, that the downdraft was less than half that of the normal cases despite much greater rainfall, and toward the end of the computation, when rainfall rate was at its peak, there was actually an updraft at low levels. Examination of streamlines suggests that in the later stages of Run 6 the vigorous circulations were strongly affected by the boundaries, and the downdrafts and updrafts below the cloud were more closely related to the continuity condition than to the water loading.

4. Growth and Decay

The growth and decay of the cloud in Runs 1, 3, and 5 are shown in Figs. 6, 7, and 8. Runs 2 and 4 so resemble Run 3 that they have been omitted. On the other hand, whereas Runs 1 and 5 resemble one another in some respects and differ in others, both are sharply differentiated from Runs 2, 3, and 4.

In all runs the value of maximum mixing ratio of liquid increased at substantially the same rate, reaching similar peaks, although that of Run 5 was somewhat smaller than the others. In Runs 2, 3, and 4, the magnitude then dropped off at a rate comparable to the previous rise, but in Runs 1 and 5 the dropoff was precipitous. Run 1 showed a leveling of maximum mixing ratio after 40 minutes, followed by a drop to zero by 53 minutes. The cloud top reached its maximum height a few minutes after the maximum value of mixing ratio, much higher in Runs 2, 3, and 4 than in Runs 1 and 5. The descent of the cloud top was at a moderate rate in Runs 2, 3, and 4, but dramatically rapid in Runs 1 and 5. This behavior again suggests that in a dynamical context, rapid, unrealistic evaporation is equivalent to increasing the rate of entrainment.

The effect of the fallout of large drops is well illustrated by the height at which maximum mixing ratio occurred. In Run 1, in which no fallout occurred, it was consistently just below the cloud top, and near the level of maximum updraft, but in the others it rose at a rate

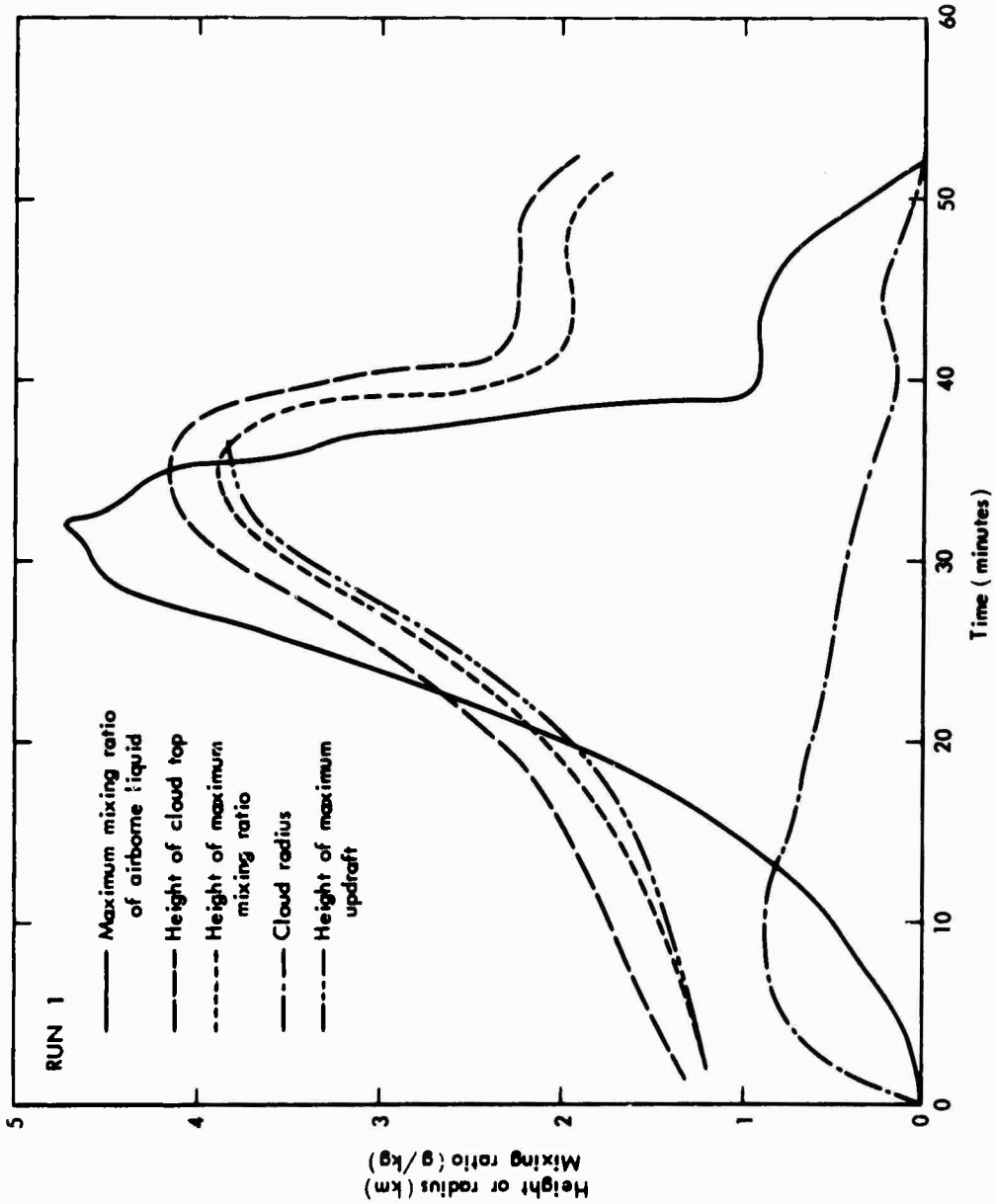

Fig. 6 -- Value of maximum mixing ratio of airborne liquid, height of maximum mixing ratio, height of maximum updraft, height of cloud top, and radius of cloud *versus* time, Run 1.

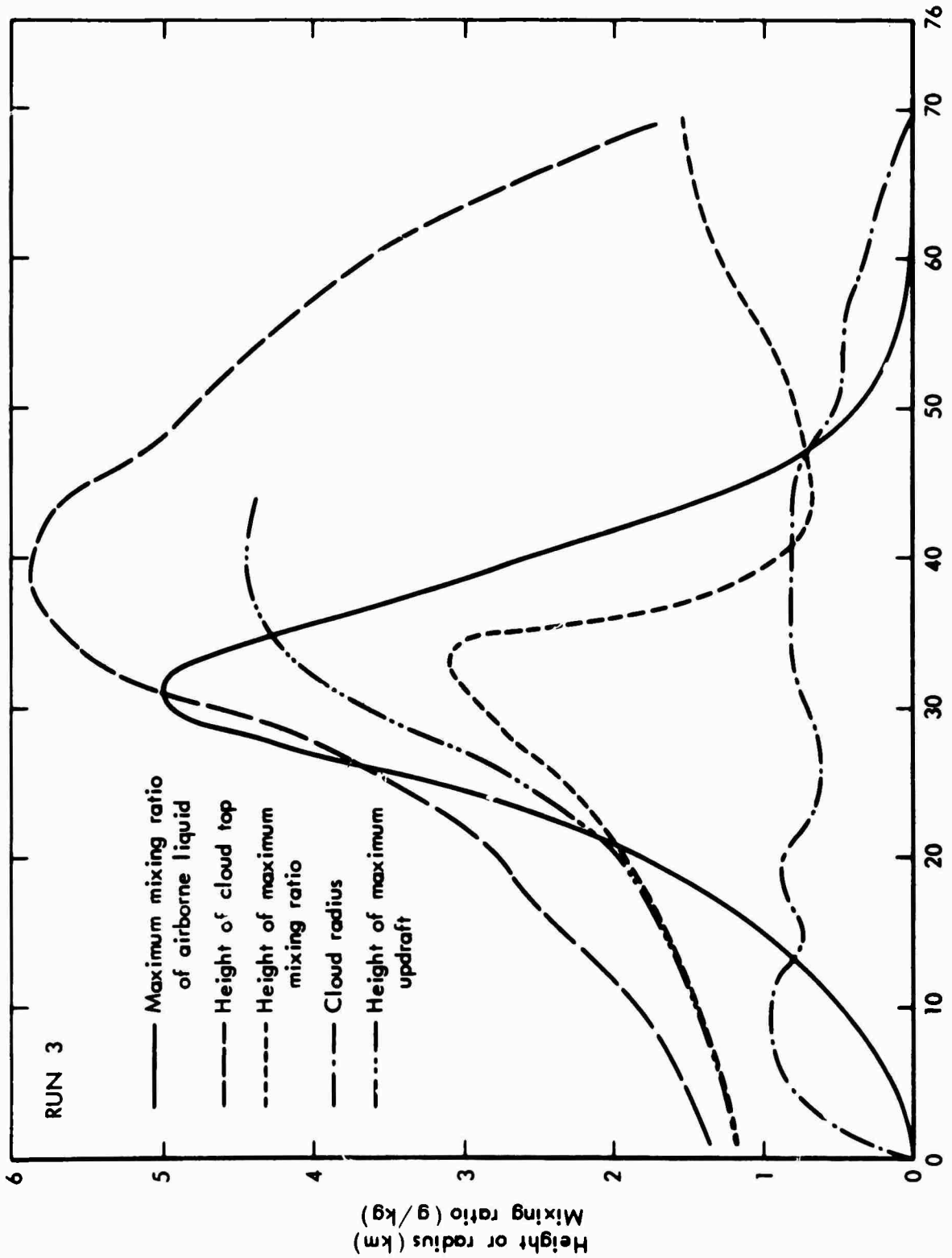

Fig. 7 -- Value of maximum mixing ratio of airborne liquid, height of maximum mixing ratio, height of maximum updraft, height of cloud top, and radius of cloud *versus* time, Run 3.

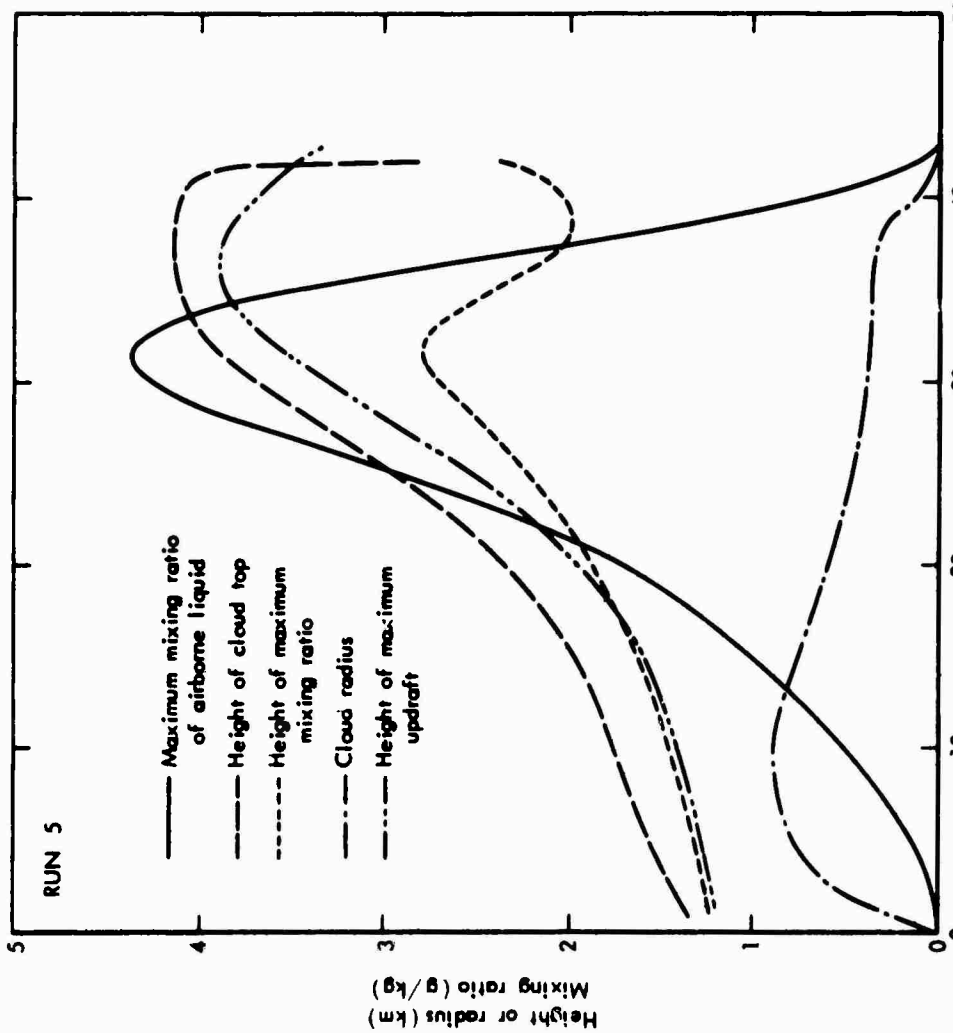

Fig. 8 -- Value of maximum mixing ratio of airborne liquid, height of maximum mixing ratio, height of maximum updraft, height of cloud top, and radius of cloud *versus* time, Run 5.

less rapid than that of the cloudtop, or even of the maximum updraft, and then started to fall before the cloudtop reached its peak. In Runs 2, 3, and 4 it fell to the lower part of the cloud, and then rose as the cloud became depleted and decayed. In Run 5 the behavior was the same, but the amount of descent was much less. From Fig. 7 one might conclude that the reduction in loading resulting from the fallout led to the increase in cloudtop height, but comparison of Figs. 6 and 8 show this not to be the case. Instead, the cooling by evaporation near the summit and on the periphery seems to be the most important process in limiting cloud height.

In the present experiments, two clouds had very limited growth, the three that incorporated realistic microphysics reached moderate heights, and one grew uncontrollably. All six reached a radius of about 800 m within five or six minutes; this appears to be related to the size and shape of the initial impulse. Thereafter, the three categories behaved quite differently. The three runs with realistic microphysics kept nearly constant radius until the final stages of the life cycle (Fig. 7). The two runs with rapid evaporation showed a steady decrease of radius after the first ten minutes or so (Figs. 6 and 8). Run 6, with normal evaporation rate but no evaporative cooling, showed a rapid increase in radius after about 15 minutes, especially near the top of the cloud. These results support the views widely held among cloud modelers that height and radius are positively correlated and that the correlation comes about as a result of greater relative entrainment of ambient air into narrower clouds than into wider ones.

Entrainment, as it is usually conceived, reduces the activity of cloud growth in several ways: one is the expenditure of energy in accelerating the entrained air (drag), and another is the decrease in buoyancy due to cooling resulting from the evaporation of cloud into the unsaturated entrained air. The former has been cited as an important term; however, the present results strongly suggest that evaporative cooling and consequent loss of buoyancy is dominant. Certainly in Run 6 more air is being entrained into the cloud than in any of the other simulations, yet growth is unchecked. This can be the consequence only of elimination of the thermal effects of evaporation, for that is

the only way in which Runs 5 and 6 differ. Runs 1 and 5, in which evaporation is rapid and its effects are quickly felt, demonstrate rapid erosion of the cloud.

5. Cloud Efficiency

Since the total amount of water that has been condensed up to a given time is known, it is possible to compute cloud efficiency as the ratio of the amount of rain to the amount of condensation. Effiency can alternatively be defined as the ratio of the amount of rain to the amount of water vapor rising through the cloud base. This definition would lead to values about half as great as those we report. Table 2 shows that even though Runs 2, 3, and 4 are closely similar in many respects, they differ greatly in cloud efficiency; this is directly related to the amount of rain since the amount of condensation is essentially the same. Run 5, however, despite a significantly smaller amount of condensation, has so much less rain than the other three that its cloud efficiency is far lower.

The growth of efficiency with time is shown in Fig. 9. The differences among Runs 2, 3, and 4 can be ascribed mainly to the rate at which suspended water is converted to precipitating water; i.e., the "autoconversion" rate. The models that encourage early conversion have less evaporation, hence earlier and more copious rain, hence higher cloud efficiency. Run 5 departs from this pattern, however, mainly because of the rapid evaporation below cloud base. When rain finally reached the ground, its initial rate of rainfall was high, so the cloud efficiency became temporarily greater than that of Run 4. But soon evaporation again took its toll, and even though the accumulated condensation was less than in the other cases, total rain was so diminished that the efficiency was very low. The vertical arrows in Fig. 9 show when rainfall ceased; it was very early in Run 5.

6. Thermal Structure

The thermal structure of the clouds is illustrated in Figs. 10, 11, and 12, which show cross sections of virtual temperature for three cases about 10 minutes before, at, and 10 minutes after the time of maximum updraft, and in Fig. 13, which shows that of Run 6 at 20 min.

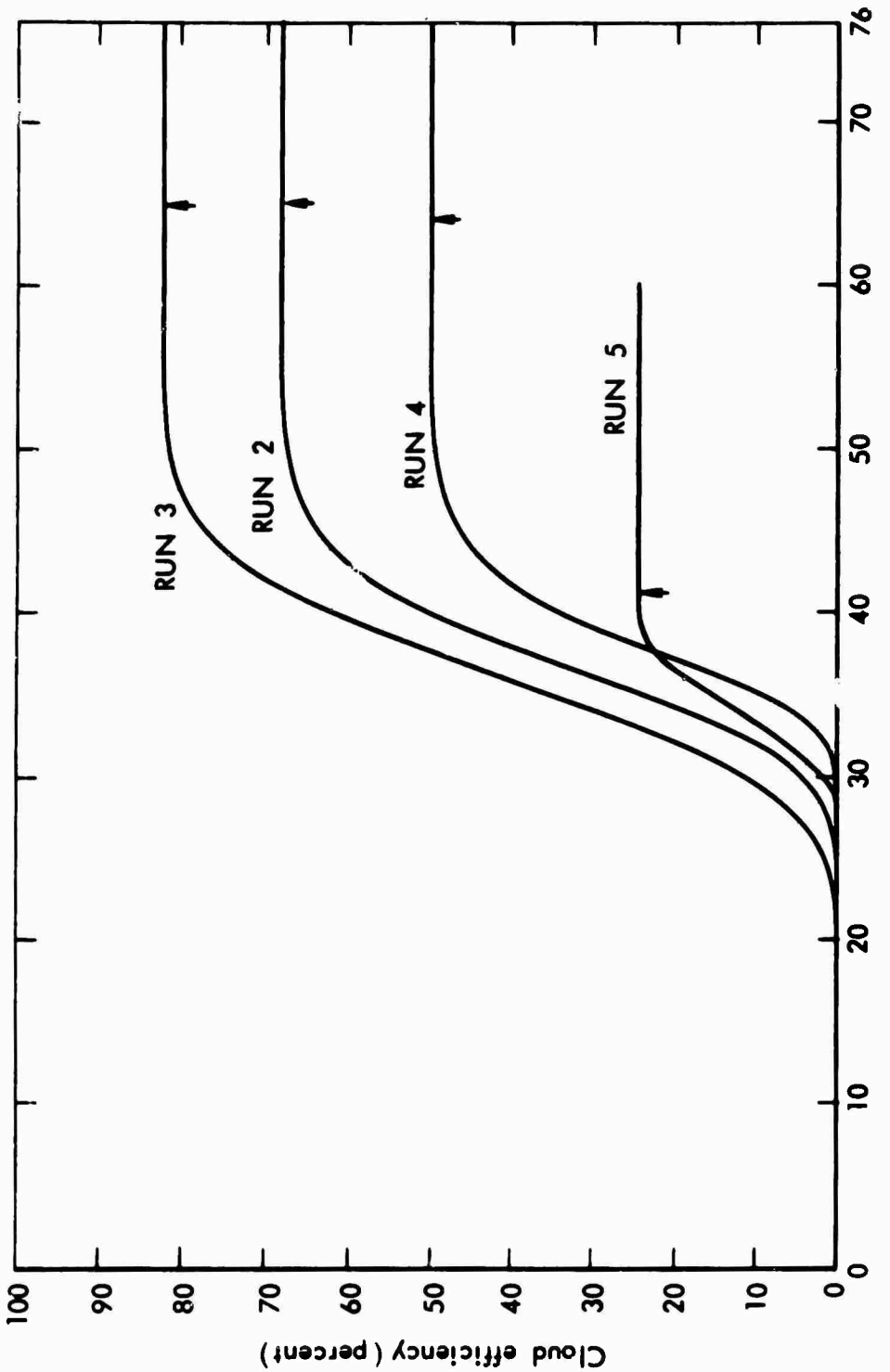

Fig. 9 -- Cloud efficiency *versus* time. Vertical arrows indicate time of cessation of rainfall at the ground.

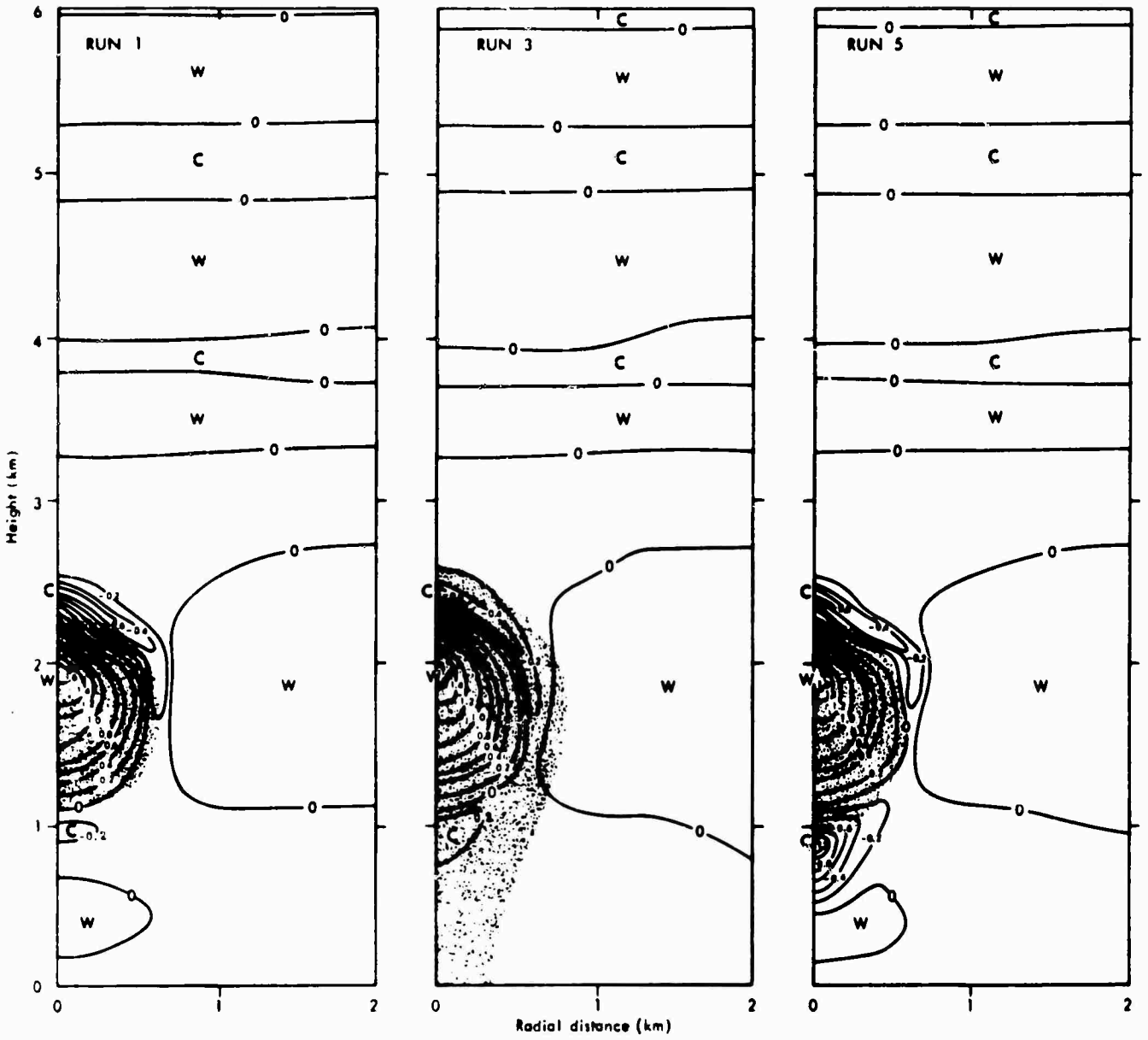

Fig. 10 -- Spatial distribution of departure of virtual temperature from its initial value, °C, at 20 minutes, for Runs 1, 3, and 5. Area with more than 0.001 g kg^{-1} airborne liquid is shaded.

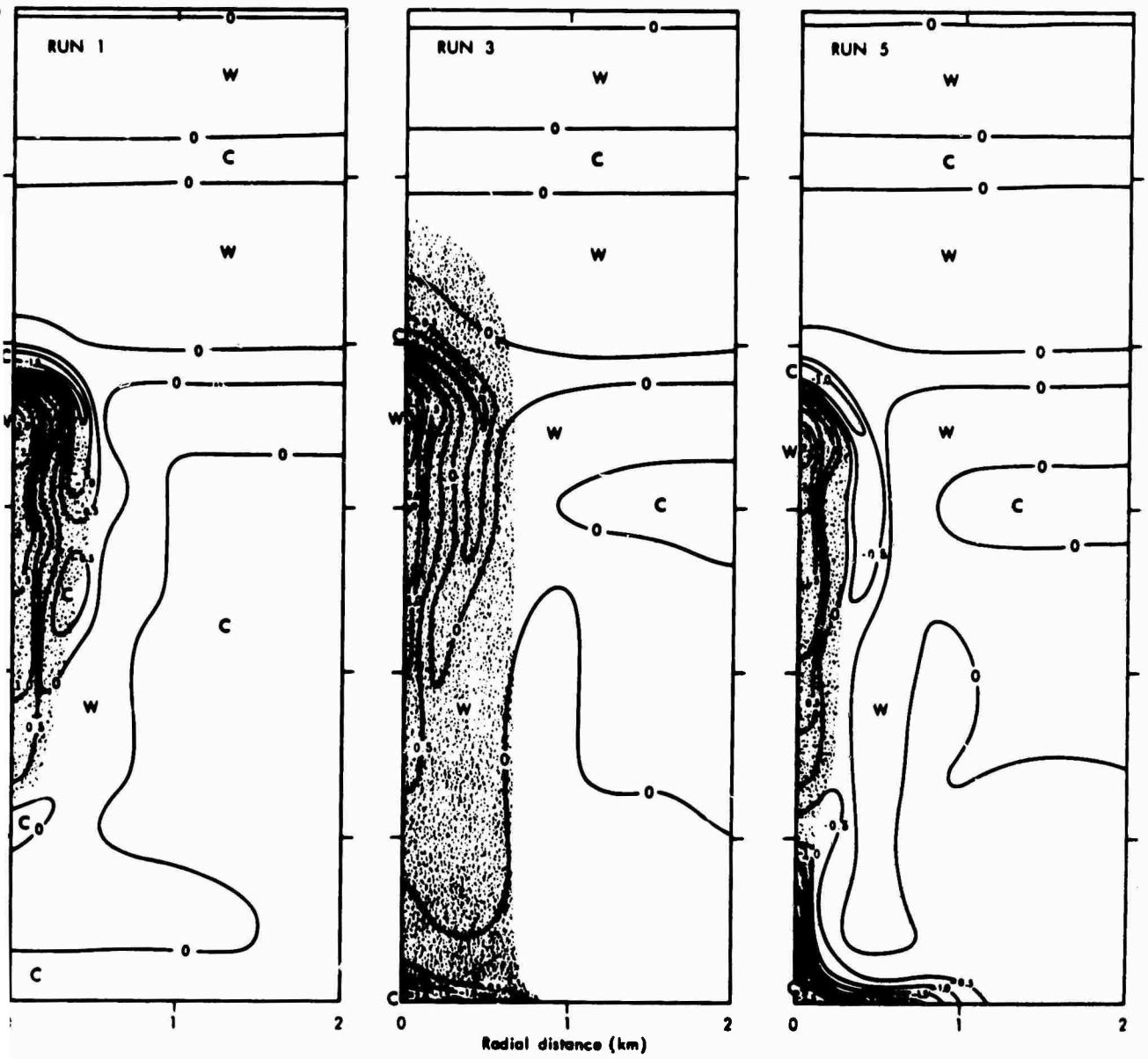

Fig. 11 -- Spatial distribution of departure of virtual temperature from its initial value, °C, at 30 minutes, for Runs 1, 3, and 5. Area with more than 0.001 g kg^{-1} airborne liquid is shaded.

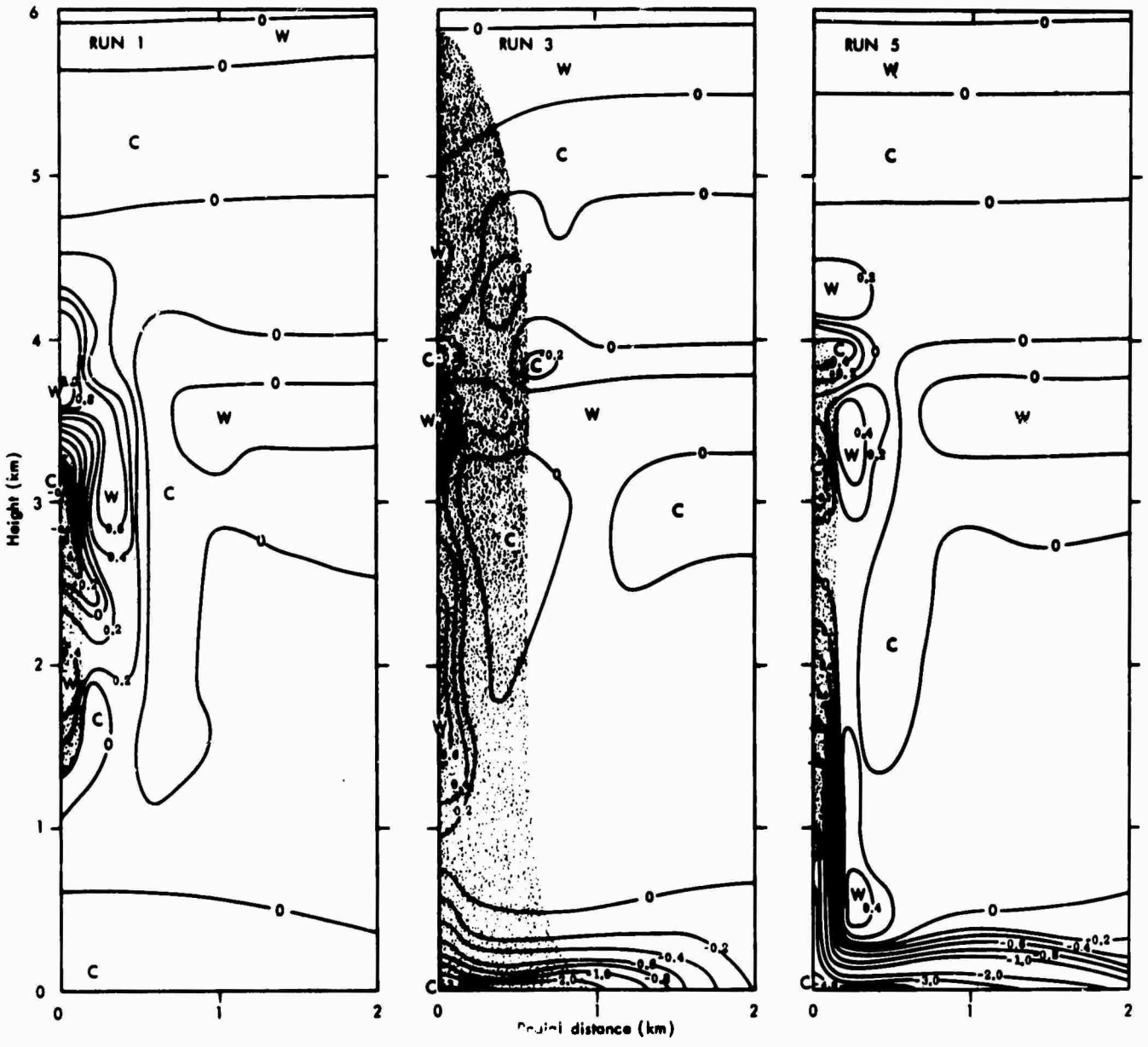

Fig. 12 -- Spatial distribution of departure of virtual temperature from its initial value, °C, at 40 minutes, for Runs 1, 3, and 5. Area with more than 0.001 g kg^{-1} airborne liquid is shaded.

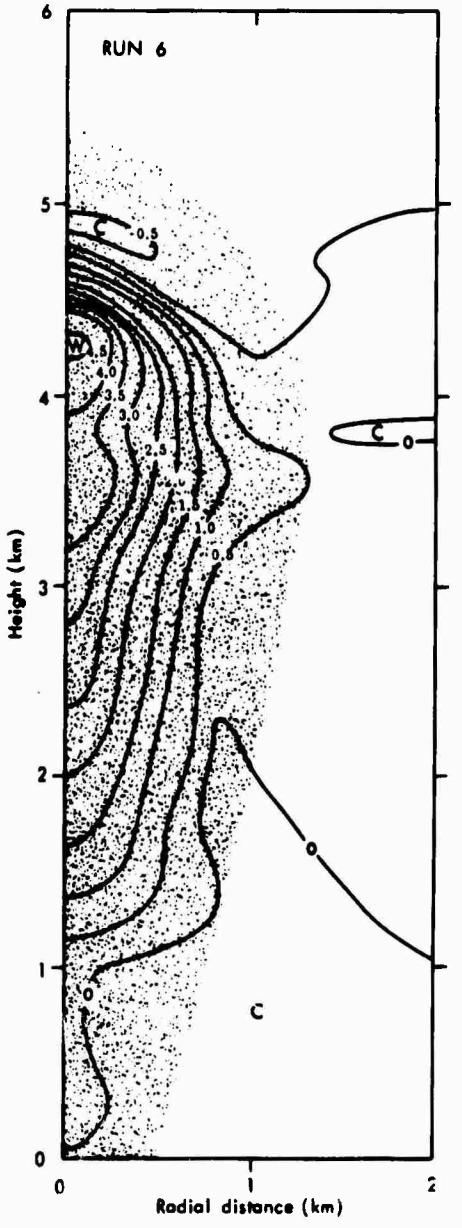

Fig. 13 -- Spatial distribution of departure of virtual temperature from its initial value, °C, at 20 minutes, for Run 6. Area with more than 0.001 g kg^{-1} airborne liquid is shaded.

The areas with more than 0.001 grams of total airborne liquid water per kilogram of dry air are shaded. It should be noted that virtual temperature is always higher than actual temperature (by about 1°C for each 6 g kg^{-1} of mixing ratio of water vapor in the present instance), and so the figures show more extensive areas of warm air than they would if actual temperature had been plotted. Virtual temperature is used here because of its direct relation with buoyancy.

The cold cap previously discussed with relation to the nonprecipitating cloud (Murray, 1970) is quite apparent in Figs. 10 and 11. Two mechanisms have been proposed to explain its existence, and it is likely that both are operative. The first is the forced lifting, and consequent dry-adiabatic cooling, of subsaturated air at the cloud summit; only this effect is permitted in Run 6. The second, and evidently more important, is evaporation. It will be noted in Figs. 10 and 11 that for the two runs with instantaneous evaporation the cold cap is outside the cloud, but with evaporation at a finite rate the cold cap is within the cloud. In Fig. 13, the cold cap is very weak despite rapid forced lifting near the cloud summit.

The effects of evaporation at the base of the cloud and at lower levels in the runs with fallout are clearly evident in the figures, as is the erosion that causes the clouds in Runs 1 and 5 to contract laterally. On the basis of the present experiments, it would appear that this lateral erosion and cooling is the most important mechanism operating to cause the dissipation of the cloud. When this erosion is strong, as in the rapid-evaporation cases, the inflow of moist air in the lower part of the cloud is effectively cut off.

At the peak of development, the warm core, even for Run 3, was very narrow. If actual rather than virtual temperature departures had been plotted, the positive departures in the cloud would have been considerably smaller, and in some instances would even have gone negative. An aircraft probing a real cloud of this nature would be in the warm core only for a short time, and might even miss it altogether. This finding is in agreement with actual reports of aircraft observations. In the period of decay, illustrated by Fig. 12, the warm core is still more elusive.

7. Autoconversion

The process of autoconversion postulated by Kessler is meant to parameterize the coalescence of small droplets to form large drops. Kessler took this to be linearly dependent on the suspended water content, with a threshold below which autoconversion does not occur; see Eq. (13). Run 2 used this conversion with Kessler's recommended threshold. Berry, by a theoretical argument, produced a formulation for autoconversion that depends on the cube of suspended water content; see Eq. (14). Berry's formulation contains as parameters the initial number concentration of droplets and their relative dispersion. Using observations from South Florida and the Caribbean, Simpson and Wiggert (1969) have proposed two sets of values for these parameters, one for clouds over water, and one for clouds over land. These they designated "maritime" and "continental." In the present study, Run 3 made use of the Berry autoconversion with the maritime parameters of Simpson and Wiggert, and Run 4 made use of the Berry autoconversion with their continental parameters. In a later paper Simpson and Wiggert (1971) used a considerably smaller value of number concentration (500 as compared with 2000), which they call the "Florida conversion." Use of this smaller number would have sped up the rate of autoconversion in Run 4, but the rate still would have been considerably slower than in Run 3. In principle many different combinations of values of the Berry parameters might be used to simulate clouds of various specific air masses.

Reference to Table 2 and Figs. 2, 3, and 4 shows that most of the results of these three runs are similar, the differences among them being much less than the differences between them and any of the other three runs. The differences that exist are easily related to the differences in autoconversion and the consequent effect on evaporation rate. Even though autoconversion commenced immediately in Runs 3 and 4, it was still of negligible amount at 10 minutes, when it commenced in Run 2. Thereafter, the precipitating water increased more rapidly with Berry-maritime than with Kessler autoconversion, eventually reaching a higher maximum. With Berry-continental autoconversion, precipitating water started its increase considerably later than the other two and never

became as great. Because of the slow conversion, Run 4 developed more suspended water than the other two, but less total airborne water. Because the rates of condensation were almost identical, this difference must be due to the greater evaporation of Run 4 associated with the larger amount of suspended water.

In comparing the Berry maritime and continental autoconversions in a one-dimensional model, Simpson and Wiggert (1969) found that the former grew a slightly taller cloud than the latter, with the difference being ascribed to a larger liquid-water content (by 1 g m^{-3}) near the summit of the continental cloud. Our results show the same difference in height, but no such difference in liquid-water content. In fact, the continental cloud in our test runs had somewhat less liquid-water content throughout than the maritime cloud. We must ascribe the difference to the larger ratio of suspended water to precipitating water in the continental model and its concomitant rate of evaporation. Evaporation resulting from entrainment is instantaneous in one-dimensional models (similar to the present Run 5). Simpson and Wiggert found that the rainfall from the maritime cloud was nearly eight times that from the continental cloud, whereas we found the ratio to be about two to one. The one-dimensional model counts as rain all water that falls from the active cloud bubble, whereas the two-dimensional model counts only the water that eventually reaches the ground. On the whole, the two-dimensional model seems to be less sensitive to changes in the computation of autoconversion than the one-dimensional model.

VI. SUMMARY AND CONCLUSIONS

The two-dimensional numerical cloud model without precipitation gives results in many respects realistic, but the addition of a precipitation mechanism, even through a highly simplified parameterization, produces significant improvement in almost all aspects of the simulation. Specifically, the precipitating model produces higher cloud tops, greater liquid-water content, and a smaller summit temperature deficit than the nonprecipitating model. Its maximum updraft is a little weaker, but the downdraft in the subcloud layer is much stronger. In shape the precipitating cloud has nearly uniform width with height, whereas the nonprecipitating cloud tends to develop a less realistic mushroom shape.

The present experiments suggest that most of the differences between the results of the several versions can ultimately be laid to evaporation. Certainly, in those characteristics in which Runs 1 and 5 resemble each other but differ from the other runs, evaporation must be the dominant factor. Chief among these characteristics is cloud height. Rapid evaporation about the summit and periphery of the cloud (which is generally associated with strong entrainment) produces a large temperature deficit, and the cold cap of relatively dense air inhibits continued cloud growth. The model with no evaporative cooling at the summit, on the other hand, developed a negligible cold cap and grew unreasonably large.

The damping effect of the cold cap in the five runs with evaporative cooling appears to be almost independent of the strength or location of the updraft. The maximum updraft occurred about the same time and altitude in all five of the runs, and was strongest in one of the fast-evaporating runs and weakest in the other. Time sections of vertical wind speed indicate that the differences in the actual maxima were smaller than is suggested by the grid-point values shown in Table 2. Such differences as occur may well be connected with evaporation in the lower part of the cloud, and in the case of the precipitating cloud, evaporation below cloud base. The six runs had marked differences in the subcloud downdraft. The nonprecipitating cloud had a negligible downdraft, the cloud with no evaporative cooling had a weak downdraft, the clouds

with normal evaporation of precipitation had moderate downdrafts, and the cloud with rapid evaporation of precipitation had a very strong downdraft. These circumstances, together with the computed liquid-water contents, strongly suggest that the major factor in developing the downdraft is not water loading but evaporative cooling.

It is of particular interest to determine the mechanisms whereby the cloud stops growing and then decays. With the sounding used in the present experiment, the simple parcel method would require a parcel displaced at the condensation level to rise to the tropopause. Typical one-dimensional models modify this by allowing the initial parcel to become progressively diluted with environment air, and so to come to rest at some moderate altitude. Such models can match the altitudes of observed clouds with impressive accuracy. The two-dimensional model is more complex in its interactions, and a full explanation of the life cycle of its simulated clouds is still not developed. However, enough information is available from these experiments to suggest an explanation of what goes on in the simulated cloud, and, it is hoped, in real clouds as well.

In this essentially Eulerian solution of the equations, no physical parcel keeps its identity from one time step to the next, and it is not strictly proper to speak of the cloud as an entity. Any grid point with more than 0.001 g kg^{-1} of liquid water is arbitrarily considered to be within the cloud, but no specific boundary surface is defined. Nevertheless, such a surface presumably exists between grid points, and it is not unrealistic to speak of the cloud as the volume enclosed by that surface.

When a suitable impulse is given to a parcel in a conditionally unstable atmosphere (in the model), the air rises, and condensation releases latent heat, causing acceleration of the vertical motion. In the two-dimensional model, a return flow is set up outside the cloud, and a supply of moist air enters both vertically and horizontally at low levels. As the active core of the cloud rises, a small circulation resembling a spherical vortex appears, and more and more the air entering the cloud is from higher and drier levels. Moreover, lifting and evaporation at the top produce a cold cap, and the cold, dry air is

brought down along the periphery, where it mixes with cloudy air to produce further evaporation and cooling. This cap of cold, dense air being dragged into the cloud eventually stops the upward motion of the cloud vortex. The altitude at which this occurs is in part a function of the rate of evaporation; thus it was high in Runs 2, 3, and 4, and low in Runs 1 and 5. In Run 6, without an effective cold cap, growth was stopped only with the cloud's arrival at the upper limit of the computational space.

Even in the nonprecipitating model, a weak counter cell appears below the cloud, and the downdraft cuts off the supply of moisture through the base. Flow into the cloud then comes from increasingly higher, generally dryer, levels. Eventually the downdraft around the periphery also cuts off the inflow of moist air from the sides, and the cloud erodes laterally, finally vanishing.

In the precipitating models, the rain falling below the original cloud base evaporates, and a relatively strong circulation cell is established with a downdraft below the cloud. Away from the cloud axis, the downdraft extends to higher levels than it does at the axis, cutting off the inflow to the lower part of the cloud, but permitting some inflow at middle levels. The downdraft around the upper periphery connected with the cold cap is, of course, less intense than in the nonprecipitating model. Thus, there is less lateral erosion, and the rain falling below the original cloud base maintains the original cloud radius because of its slow rate of evaporation. After about 30 minutes, even in the precipitating models, all inflow is effectively cut off, and thereafter the cloud decays. If there is no evaporative cooling, however, the cloud does not erode. In fact, as the cloud approaches the ceiling, it grows in radius. This is probably a consequence of the distortion in flow patterns caused by the rigid boundaries, as is the appearance and subsequent disappearance of a downdraft below the cloud.

A somewhat puzzling result of the present experiment was that in all six runs, regardless of their microphysics, the maximum updraft, which signalizes the dynamic peak of cloud development, occurred at 30 minutes. Previous experience (Murray, 1971) suggests that this time is a function of the basic sounding and of the nature of the initial

impulse. There may be other influences at work, however, and further study of this feature is indicated.

The principal deficiency of the model as it now stands is its failure to treat the ice phase. Work is now in progress to incorporate a parameterization of processes involving ice crystals. This should make the model not only more realistic, but more useful for studying cloud modification.

REFERENCES

Àrnason, G., P. S. Brown, and R. T. Chu, 1969: "Numerical simulation of the macrophysical and microphysical processes of moist convection," *Proceedings of the WMO/IUGG Symposium on Numerical Weather Prediction in Tokyo*, 26 November- 4 December 1968, pp. I-11 - I-21.

Àrnason, G., R. S. Greenfield, and E. A. Newburg, 1968: "A numerical experiment in dry and moist convection including the rain stage," *Journal of the Atmospheric Sciences*, Vol. 25, No. 3, pp. 404-415.

Berry, Edwin X , 1968: "Modification of the warm rain process," *Proceedings of the First National Conference on Weather Modification*, Albany, 28 April-1 May 1968, pp. 81-88.

Gunn, Ross, and Gilbert D. Kinzer, 1949: "The terminal velocity of fall for water droplets in stagnant air," *Journal of Meteorology*, Vol. 6, No. 4, pp. 243-248.

Kessler, Edwin, 1967: *On the Continuity of Water Substance*, Technical Memorandum IERTM-NSSL 33, ESSA National Severe Storms Laboratory, Norman, Oklahoma, 125 pp.

Kessler, Edwin, 1969: "On the distribution and continuity of water substance in atmospheric circulations," *Meteorological Monographs*, Vol. 10, No. 32, 84 pp.

Koenig, L. R., 1966: "Numerical test of the validity of the drop-freezing/splintering hypothesis of cloud glaciation," *Journal of the Atmospheric Sciences*, Vol. 23, No. 6, pp. 726-740.

Liu, J. Y., and H. D. Orville, 1969: "Numerical modeling of precipitation and cloud shadow effects on mountain-induced cumuli," *Journal of the Atmospheric Sciences*, Vol. 26, No. 6, pp. 1283-1298.

Malkus, J. S., and G. Witt, 1959: "The evolution of a convective element: a numerical calculation," *The Atmosphere and the Sea in Motion*, Rockefeller Institute Press and Oxford University Press, New York, pp. 425-439.

Marshall, J. S., and W. McK. Palmer, 1948: "The distribution of raindrops with size," *Journal of Meteorology*, Vol. 5, No. 4, pp. 165-166.

Murray, F. W., 1970: "Numerical models of a tropical cumulus cloud with bilateral and axial symmetry," *Monthly Weather Review*, Vol. 98, No. 1, pp. 14-28.

Murray, F. W., 1971: "Humidity augmentation as the initial impulse in a numerical cloud model," *Monthly Weather Review*, Vol. 99, No. 1, pp. 37-48.

Ogura, Yoshimitsu, 1962: "Convection of isolated masses of a bouyant fluid: a numerical calculation," *Journal of the Atmospheric Sciences*, Vol. 19, No. 6, pp. 492-502.

-----, 1963: "The evolution of a moist convective element in a shallow, conditionally unstable atmosphere: a numerical calculation," *Journal of the Atmospheric Sciences*, Vol. 20, No. 5, pp. 407-424.

Simpson, Joanne, and Victor Wiggert, 1969: "Models of precipitating cumulus towers," *Monthly Weather Review*, Vol. 97, No. 7, pp. 471-489.

-----, 1971: "1968 Florida cumulus seeding experiment: Numerical model results," *Monthly Weather Review*, Vol. 99, No. 2, pp. 87-118.

Simpson, J., R. H. Simpson, D. A. Andrews, and M. A. Eaton, 1965: "Experimental cumulus dynamics," *Reviews of Geophysics*, Vol. 3, No. 3, pp. 387-431.

Srivastava, R. C., 1967: "A study of the effect of precipitation on cumulus dynamics," *Journal of the Atmospheric Sciences*, Vol. 24, No. 1, pp. 36-45.

Weinstein, A. I., 1969: "A numerical model of cumulus dynamics and microphysics," *Journal of the Atmospheric Sciences*, Vol. 27, No. 2, pp. 246-255.

Wobus, H. B., F. W. Murray, and L. R. Koenig, 1971: "Calculation of the terminal velocity of water drops," *Journal of Applied Meteorology*, Vol. 10 (to be published in August 1971).